

RESEARCH PAPER

Rutin: a Flavonoid Precursor for Synthesis of ZnFe₂O₄ Nanoparticles; Electrochemical Study of Zinc Ferrite-chitosan Nanogel for Doxorubicin Delivery

Mostafa Shafiee¹, Salar Hafez Ghoran^{1,2,*}, Sadegh Bordbar³, Mina Gholami¹, Moslem Naderian⁴, Fatemeh Sadat Dehghani¹, Ali Mohammad Amani^{1,7}

¹ Department of Medical Nanotechnology, School of Advanced Medical Sciences and Technologies, Shiraz University of Medical Sciences, Shiraz, Iran

² Department of Chemistry, Faculty of Science, Golestan University, Gorgan, Iran

³ Department of Chemical Engineering, Isfahan University of Technology, Isfahan, Iran

⁴ Department of Pharmacognosy, School of Pharmacy, Shiraz University of Medical Sciences, Shiraz, Iran

ARTICLE INFO

Article History:

Received 14 August 2020

Accepted 05 December 2020

Published 01 January 2021

Keywords:

As-synthesized ZnFe₂O₄ NPs

Chitosan

Doxorubicin

Drug delivery

Ruta graveolens L

Rutin

ABSTRACT

The use of core-shell nanoparticles as controlled drug delivery vehicles has proven successful, yet their production and application require costly and toxic chemicals. We hereby use a natural glycosylated flavonoid (rutin) for synthesis of a nanocarrier for doxorubicin delivery. For this target, a convenient two-step synthesis was processed including a synthesis of bio-zinc ferrite nanoparticles without N₂ gas and chitosan coating (CS; bio-zincferrite@chitosan). The as-synthesized magnetic nanogel was characterized using scanning electron microscopy (SEM), transmission electron microscopy (TEM), Fourier transformed infrared (FT-IR) spectroscopy, and electro-analytical methods including cyclic voltammetry and electrochemical impedance spectroscopies. The collapse/swell potential of the coated CS layers of the bio-NPs were found to be responsible for the observed pH dependence of doxorubicin delivery. Results exhibited the drug release of bio-nanogel can be induced at pH ranging from 6 to 7. Therefore, capacity and efficiency parameters of the anti-cancer drug onto the NPs were obtained as equal to 43.5% and 78.6%. The present work provides a simple method to fabricate smart pH-responsive nanogel for cancer therapy.

How to cite this article

Shafiee M., Hafez Ghoran S., Bordbar S., Gholami M., Naderian M., Dehghani F.S., Amani A.M. Rutin: a Flavonoid Precursor for Synthesis of ZnFe₂O₄ Nanoparticles; Electrochemical Study of Zinc Ferrite-chitosan Nanogel for Doxorubicin Delivery. J Nanostruct, 2021; 11(1): 114-124. DOI: 10.22052/JNS.2021.01.013

INTRODUCTION

In recent decades, green synthesis of nanoparticles using plant extract is a new, inexpensive, and environmentally friendly method. The size and structure of the NPs could easily manipulated by using different concentrations and reaction conditions including light, temperature, pH, etc. [1, 2]. Synthesized iron oxide NPs by either plant

extracts or small molecules are depending on the plant type, which influences the biological, physical, and chemical properties. Associated with the diverse biological applications, this has interestingly encouraged the researchers to follow up the new resources like plant species [3]. The important process in the synthesis of zinc ferrite NPs is being low cost and high efficiency for large-scale industrial production. The magnetic and biological

* Corresponding Author Email: S_Hafezghoran@yahoo.com
Aliamani@sums.ac.ir

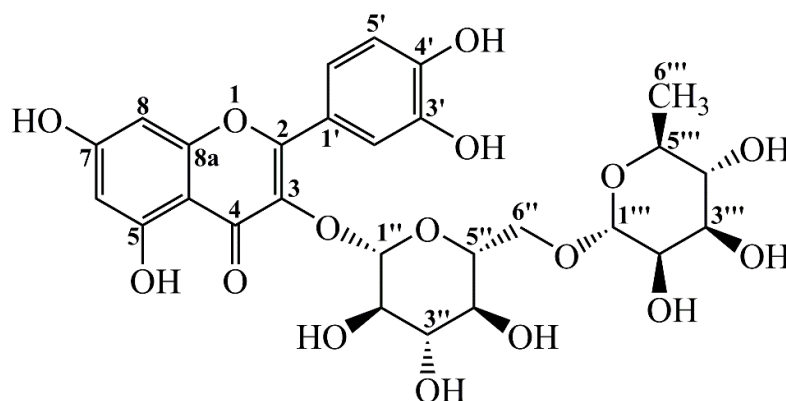


Fig. 1. Chemical structure of rutin isolated from the *Ruta graveolens* L. leaves.

properties of Fe_3O_4 can be fluctuated by stoichiometric and crystalline structure. Most important factor affecting the magnetization and stability of the magnetic property of iron magnet NPs is the replacement of other metal cations within the iron magnet structure [4, 5]. Another advantage of using magnetic NPs as drug carriers over traditional chemotherapy is that NPs penetration and further accumulation in the anywhere of body can be potentially guaranteed the treatment of all types of tumors by specific drug delivery in the body, causing the reduction of undesirable side effects. Likewise, these nanoparticle beads will be ideal for using in molecular biology and nano-medical applications because of some important attitudes such as physicochemical properties, size, manageable form, colloidal stability and spontaneous bio-degradation [6]. Addition of metals such as Zinc, Cobalt, Platinum, Nickel, and Manganese to magnetite, results in changes in magnetization. Recent studies have shown that small amounts of zinc substitution can increase the saturation magnet. To this respect, the use of zinc ferrite magnetite leads to easy control of magnetic properties when compared to Fe_3O_4 [7, 8]. Ferrite magnetites can be functionalized with polymer coatings thereby, the levels of responsiveness is enhanced. In addition to increasing the number of active agent groups on the surface, it practically provides a matrix, which is sensitive to pH, temperature, light, etc. Chitosan, for instance, a multifunctional natural polysaccharide composed of chitin unit bearing $-\text{OH}$ and $-\text{NH}_2$ groups, shows desirable efficiency in the removal of Azo dyes. Moreover, smart polymers can modify the magnetite ferrite structures, a proven ability to overcome against

multidrug-resistance on drug-resistance cancer [9-12]. The amino functionality binds to a metal oxide either by adsorption or covalent bonding. Therefore, the chitosan amine residue can be exploited for derivatization with biomolecules, drugs and metals [13, 14].

The main objective of the present study was the synthesis of chitosan-coated ZnFe_2O_4 NPs using a flavonoid precursor, rutin, isolated from *Ruta graveolens* L. leaves (Fig. 1) together with the efficiency of doxorubicin and siRNA delivery. For the characterization, we used several techniques including ultraviolet-visible (UV-Vis) absorption spectroscopy, transmission electron microscopy (TEM), scanning electron microscopy (SEM), energy-dispersive X-ray spectroscopy (EDS), X-ray diffraction (XRD), vibrating sample magnetometer (VSM), Fourier transform infrared (FT-IR) spectroscopy, and thermogravimetric analysis (TGA).

MATERIAL AND METHODS

Material and instruments

All organic solvents including n-hexane, chloroform (CHCl_3), ethyl acetate (EtOAc), acetone, methanol (MeOH), were commercially purchased and applied without any further purification. Doxorubicin hydrochloride was purchased from Cayman chemical (Ann Arbor, MI, USA), Chitosan low molecular weight; CAS number: 9012-76-4, $[\text{Zn}(\text{CH}_3\text{COO})_2] \cdot 2\text{H}_2\text{O}$, $\text{FeCl}_3 \cdot 6\text{H}_2\text{O}$, and $\text{FeCl}_2 \cdot 4\text{H}_2\text{O}$ were purchased from Sigma-Aldrich.

Plant material, extraction and isolation

The leaves of *R. graveolens* L. were collected from botanical garden of *University of Tabriz*, Iran in 2018. A voucher specimen (No. 2874) was de-

posited in the herbarium of the *University of Shiraz* (Shiraz, Iran). The air-dried and powdered leaves of *R. graveolens* (300 g) was extracted with 3 L of 80% methanol (3 × 1 L) by ultra-sonication for 1 hour. The extract was carefully filtered through Whatman filter paper and lyophilized on a rotary evaporator before being redissolved in 500 mL distilled water and defatted with 500 mL *n*-hexane in a separation funnel. In order to eliminate the semi-polar compounds, the aqueous layer was then fractionated with chloroform. After careful partitioning, the water-soluble portion was stored in refrigerator for 72 hours; a yellowish precipitate separated out of the solution. The afforded precipitate was washed successively with chloroform, ethyl acetate, acetone and methanol. The remained material was evaporated under reduced pressure using rotary evaporator to dryness to yield 1.376 g yellow powder (rutin also called as rutoside).

Identification of isolated rutin

To determine whether rutin have been purified, filtered yellow powder was compared with standard rutin using analytical HPLC equipped by column (Lichrosphere-100, RP C-18, 250 × 4.6 mm ID, 5 μm with precolumn) and mobile phase of acetonitrile:water (60:40 ratio) with a flow rate of 1 mL.min⁻¹ and detected at 284 nm [15]. Afterwards, its structure was confirmed using NMR experiment (¹H- & ¹³C-NMR data) compared with the previous published literature [16].

Synthesis of Zinc ferrite nanoparticles using rutin

Zinc ferrite NPs were synthesized by co-precipitation method reported by Hafez Ghoran et al. [17]. First 1.3 g of FeCl₂.4H₂O, 5.4 g of FeCl₃.6H₂O, and 0.8 g [Zn(CH₃COO)₂].2H₂O were dissolved in 30 mL deionized water with vigorous stirring. Then, as reductive precursor, 70 mL of rutin (C₂₇H₃₀O₁₆; 0.1 mM concentration; pH=11), heated at 65°C, was quickly added into the mixture and magnetically stirred. In order to reach the pH of 9, the 25% solution of NH₃ was gradually added for 2 hours and temperature was maintained at 65°C. The mixture turned into a dark brown color, indicating the ferrite formation and allowed to cool down at room temperature. Washing was carried out to remove chloride ions impurities with distilled water and acetone, respectively. As-synthesized zinc ferrite nanoparticles were washed several times and then left in an electric oven for 48 hours at 55°C to eliminate water.

Coating the nanoparticles with Chitosan

Briefly, 0.5 g of synthesized zinc ferrite nanoparticles was added into the 50 mL solution of acetic acid (1%) which is containing 0.12 g of chitosan and magnetically stirred. Thereafter, 100 μL of (3-Aminopropyl)triethoxysilane (APTES) was added to the mixture in order to increase the reactions' pH followed by using 50 mL of 1 molar solution of Sodium Hydroxide. The reaction was stayed for 4 hours at 50°C and then heating was turned off for 24 hours in order to obtain the better cross-link. Finally, the coated nanoparticles were filtered and washed several times with distilled water and dried in an overnight [18].

In vitro Doxorubicin loading/release

In order to investigate the drug loading/release, doxorubicin (DOX) was selected as a model drug and loaded on ZnFe₂O₄ NPs [19]. Solutions of different concentrations of doxorubicin were prepared in PBS buffer. The pH values of the solutions were adjusted to 7.4, 6.4 and 5.2, respectively, using HCl. The electrochemical cell consisted of glassy-carbon working electrode, a Pt wire counter electrode, and an Ag/AgCl reference electrode. The electrochemical measurements were carried out in the acetate buffer at pH 5.2 and the square-wave voltammograms were recorded between -0.2 V and -0.8 V.

Doxorubicin Loading

50 mg of chitosan-coated ZnFe₂O₄ NPs was added to an aqueous solution of DOX (50 mL, 1.0 mg mL⁻¹) at 37 °C in the dark and stirred for 24 h. Then, the obtained DOX-loaded ZnFe₂O₄-chitosan was collected and rinsed with PBS to remove the surface physisorbed DOX molecules. The supernatant liquid was used for loading content calculating. The obtained precipitate was isolated for releasing experiment.

Doxorubicin Release

To explore the pH-dependent release of DOX from the chitosan-coated ZnFe₂O₄ NPs and simulate the physiological conditions of tumor cells and healthy body fluids, two PBS solutions with two different pH values, i.e. 6.4 and 7.4, respectively, were prepared. The DOX-loaded ZnFe₂O₄-chitosan was added to a PBS buffer at pHs, 7.4, 6.4, and 5.2. The concentration of free doxorubicin released from the carrier into the solutions was then measured with the square wave voltammetric sensor.

At desired time intervals, 5 mL of PBS solution was taken out to determine the amount of released DOX by SWV. For each measurement, the total volume of stock solution was fixed by immediate adding 5 mL fresh buffer back.

Characterization of samples

Analytical HPLC (Knauer Co., Germany) and the nuclear magnetic resonance (NMR; Bruker Biospin GmbH spectrometer; ^1H at 300 MHz and ^{13}C at 75 MHz) spectra were applied for identification of rutin. The as-synthesized NPs were characterized using a series of instrumental techniques including Fourier transform infrared (FTIR) by Perkin-Elmer spectrometer in KBr tablets, X-ray diffraction (XRD) patterns by a PANalytical X'Pert Pro (UK) using Ni-filtered Cu Ka radiation, Scanning electron microscopy (SEM) images by Philips XL30 equipped with an energy dispersive X-ray spectroscopy, transmission electron microscopy (TEM) images by ZEISS 10A conventional TEM model Carl Zeiss-EM10C-100 KV (Germany), magnetic properties by vibrating-sample (VSM, LBKFB, Maghnatis Daghigh. Kavir Co) magnetometer, thermogravimetric analysis (TGA) by using Q50 model (TA instruments, USA), ultra violet-visible (UV-Vis) by Varian, model; Carry 100 in a range between 200-800 nm, voltammetric experiments by Origa-flex500 potentiostat (Origalys, France), and a pH meter for pH measurements.

RESULTS AND DISCUSSION

Characterization of isolated rutin from *R. graveolens* L.

Ruta graveolens L. (belongs to Rutaceae family) commonly called as "Sodab" in Persian, which is cultivated in different parts of Iran [20]. The most abundant flavonoid glycoside naturally occurring in the *R. graveolens* L. (Garden Rue) is rutin (quercetin-3-O- β -D-rutinoside or rutoside). It can be used as a natural precursor for synthesis of magnetic NPs, which is currently of interest. Flavonoid skeleton of rutin brings about several magnificent pharmacological features such as antioxidant, antibacterial, antiulcer, antitumor, anti-inflammatory, anti-hyperglycemia, analgesic, anti-hyperlipidemia, anticancer, myocardial protecting and hepatoprotective activities [21, 22]. In the following, the Nuclear Magnetic Resonance (NMR) data of rutin are mentioned.

NMR Spectroscopic data

Rutin (Rutoside/Quercetin-3-O- β -D-rutinoside), obtained as a yellow powder with molecular formula of $\text{C}_{27}\text{H}_{30}\text{O}_{16}$. ^{13}C NMR (75 MHz, in Pyridine- d_5): Flavonol core; δ_{C} 178.69 (C-4), 165.97 (C-7), 162.65 (C-5), 158.15 (C-2)*, 157.78 (C-8a)*, 150.50 (C-4'), 146.33 (C-3'), 135.39 (C-3), 122.99 (C-6'), 122.34 (C-1'), 117.62 (C-2'), 116.13 (C-5'), 104.64 (C-4a), 99.26 (C-6), 94.72 (C-8); Sugar moiety (rhamnopyranosyl); 104.81 (C-1''), 76.00 (C-2''), 77.39 (C-3''), 71.34 (C-4''), 78.52 (C-5''), 68.47 (C-6''), 102.28 (C-1'''), 72.17 (C-2'''), 72.73 (C-3'''), 73.35 (C-4'''), 69.80 (C-5'''), 18.26 (C-6'''). ^1H NMR (300 MHz, in Pyridine- d_5): Flavonol core; δ_{H} 13.45 (1H, s, 5-OH), 8.24 (1H, d, $J = 2.2$ Hz, H-2'), 8.01 (1H, d, $J = 8.6, 2.2$ Hz, H-6'), 7.37 (1H, d, $J = 8.6$ Hz, H-5'), 6.89 (1H, d, $J = 2.1$ Hz, H-8), 6.81 (1H, d, $J = 2.1$ Hz, H-6); Sugar moiety (rhamnopyranosyl); 6.28 (1H, d, $J = 7.4$ Hz, H-1''), 4.25 (1H, dd, $J = 8.5, 7.4$ Hz, H-2''), 4.18 (1H, dd, $J = 8.8, 8.5$ Hz, H-3''), 4.03 (1H, dd, $J = 8.8, 7.3$ Hz, H-4''), 4.30 (1H, m, H-5''), 4.52 (1H, m, H-6''a), 3.97 (1H, m, H-6''b), 5.41 (1H, d, $J = 6.9$ Hz, H-1'''), 4.44 (1H, dd, $J = 8.4, 6.9$ Hz, H-2'''), 4.41 (1H, dd, $J = 8.8, 8.4$ Hz, H-3'''), 4.10 (1H, dd, $J = 8.8, 7.4$ Hz, H-4'''), 4.21 (1H, m, H-5'''), 1.49 (3H, d, $J = 6.9$ Hz, H-6'''). *Interchangeable values; [16].

Synthesis of ZnFe_2O_4 nanoparticles using rutin

Adding the degassed ions including Fe^{3+} , Fe^{2+} , and Zn^{2+} to 0.1 mM of rutin solution (pH= 11) is caused to formation of tri-complex rutin in media. This phenomenon was recognized as the main factor for removing the neutral gas, N_2 , during the reaction procedure. Meanwhile, when pH is increased through NH_3 treatment, the metal-ligand complexes will be unstable and consequently led to the green synthesis of rutin- ZnFe_2O_4 NPs (Fig. 2).

Fourier transform infrared spectroscopy

Fig. 3 illustrates the FT-IR spectra of chitosan and biosynthesized chitosan-coated ZnFe_2O_4 NPs, respectively, which were recorded in the range of 400–4000 cm^{-1} . In general, the IR data of rutin's chitosan-coated ZnFe_2O_4 NPs displayed a band 1621 indicating an interaction of the Zn^{2+} via the carbonyl (C-4) [23]. In chitosan spectrum, peaks at 1646 cm^{-1} and 1328 cm^{-1} indicate the presence of residual *N*-acetyl groups, which are approved the

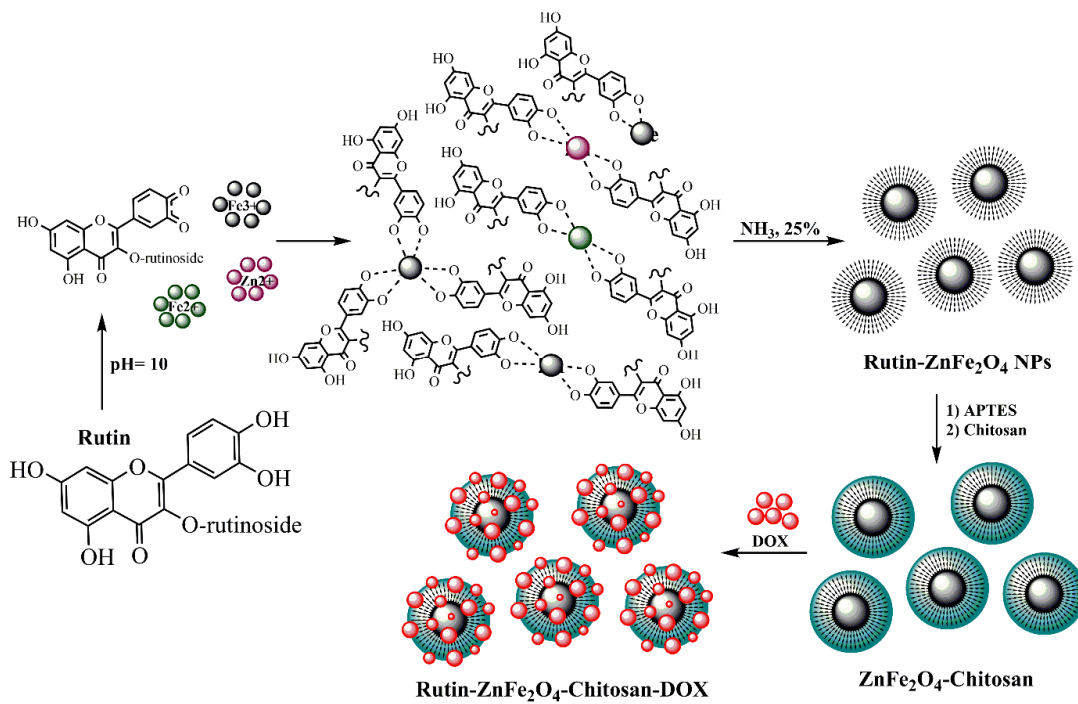


Fig. 2. General overview of green synthesis of rutin-ZnFe₂O₄-chitosan-DOX NPs.

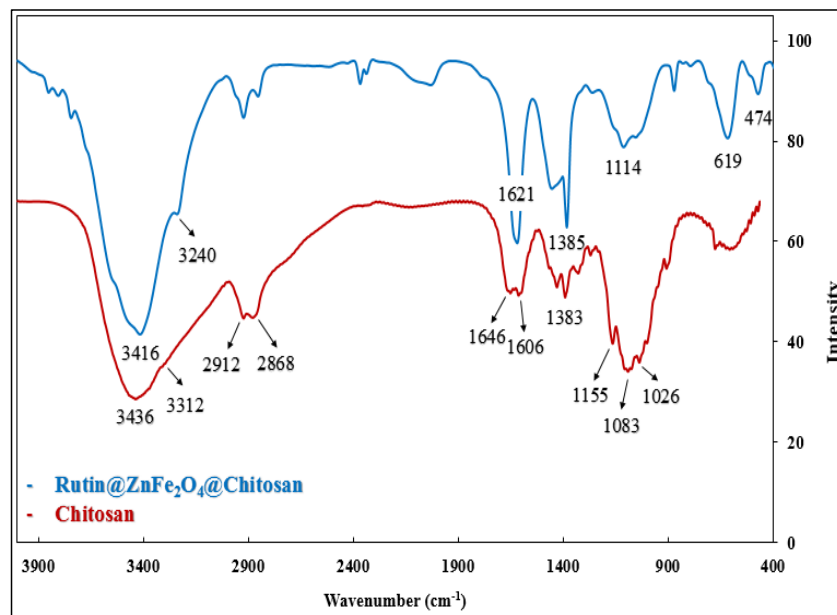


Fig. 3. FTIR spectra of chitosan (red graph) and chitosan-coated ZnFe₂O₄ NPs (blue graph).

C=O stretching bands of amide I and C-N stretching bands of amide III, respectively [24]. In respective manner, shifting peaks to 1621 cm⁻¹ and 1385 cm⁻¹ of the biosynthesized NPs spectrum ascertain the hydrogen bonding of chitosan in the blend as

well. A wide band in the 3436 cm⁻¹ is related to N-H stretching, O-H stretching and the intermolecular hydrogen bonds of chitosan. However, the presence of APTES molecules, as cross linkers, is significantly documented by vibrational enlarge-

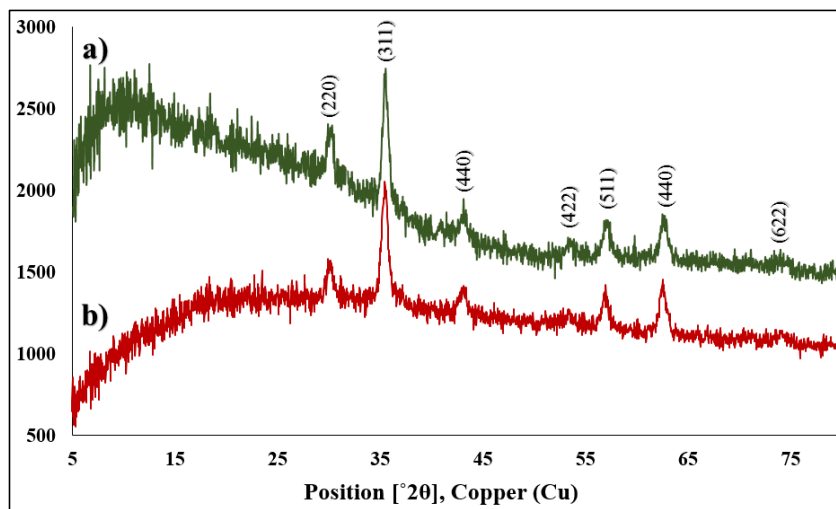


Fig. 4. XRD spectra of ZnFe_2O_4 NPs (a) and chitosan-coated ZnFe_2O_4 NPs (b).

ment of both the primary amine (NH) and OH stretching groups. In this respect, a slight shift of the OH band (3416 cm^{-1} for 3436 cm^{-1}) accompanied by the elongation and suppression of band 3312 cm^{-1} is observed. This may also be due to the interaction of silicon (Si) and OH [25]. The absorption bands at 2912 cm^{-1} and 2868 cm^{-1} are assigned to the $-\text{CH}_3$ and $-\text{CH}_2-$ residues in chitosan structure and the peak at 1383 ascribes to $-\text{C}-\text{O}$ stretching of primary alcoholic group of chitosan. The peak shift to the lower wavelength (3416 cm^{-1}) is likely owing to hydrogen bonding in the blend of nanoparticles. In the FTIR spectrum of rutin- ZnFe_2O_4 -chitosan, compared with the spectrum of chitosan, the 1646 cm^{-1} and 1606 cm^{-1} peaks of N-H bending vibration shifted to the lower frequency, 1621 cm^{-1} , are related to the reaction of the blend, which confirms the magnetic ZnFe_2O_4 NPs was coated by chitosan. Accordingly, the main cause of disappearing bands at 1026 cm^{-1} , 1083 cm^{-1} , and 1155 cm^{-1} in chitosan corresponding to the C-O stretching, and asymmetric stretching of the C-O-C bridge, respectively [26, 27]. Moreover, the FTIR spectrum of rutin- ZnFe_2O_4 -chitosan reveals the formation of spinel structured ZnFe_2O_4 . Two typical IR absorption bands, 474 cm^{-1} and 619 cm^{-1} , assign to the inverse spinel ferrite structure. The former indicates the stretching vibration of tetrahedral groups $\text{Zn}^{2+}\text{O}^{2-}$ and the latter represents the octahedral group complex $\text{Fe}^{3+}\text{O}^{2-}$ [28].

XRD analysis

The XRD patterns of the rutin- ZnFe_2O_4 and

rutin- ZnFe_2O_4 -chitosan are indicated in Fig. 4. The presence of (220), (311), (440), (422), (511), (440), and (622) peaks in the XRD pattern of bio-synthesized zinc ferrite NPs (Fig. 4a) are in accordance with a single-phase cubic spinel structure [29], which is in agreement with JCPDS standard cards no. 1012-22 with no extra impurity phases. The average crystalline size was estimated by the Scherrer equation, , from the X-ray peak broadening (FWHM; full-Width at half maximum) of the main peak (311), where λ is the wavelength of Cu K-alpha (1.79 \AA), ϑ_b is the angle of Bragg diffraction, and $\beta = B - b$. B is the full FWHM ($0.58^\circ 2\theta$) and b related to the instrumental line broadening [30]. On the whole, the crystalline size of biosynthesized ZnFe_2O_4 NPs was measured as about 17 nm using this equation. Fig. 4b also revealed that the ZnFe_2O_4 NPs coated by chitosan contain the ZnFe_2O_4 .

Morphological investigation

Fig. 5a-e illustrates SEM image of ZnFe_2O_4 NPs at different magnifications that agree with the theoretical results measured by the Debye-Scherrer's equation applied for estimation of average crystal sizes. TEM images with various magnifications were also evaluated for the morphology of biosynthesized magnetic nanoparticles (Fig.s 5f-i). Fig. 5g shows that ZnFe_2O_4 NPs are somewhat polydisperse and spherical shape with the average particle size of 18-32 nm, but strongly aggregated. The less agglomerated chitosan-coated ZnFe_2O_4 NPs, which can be seen in Fig. 5i, might be related

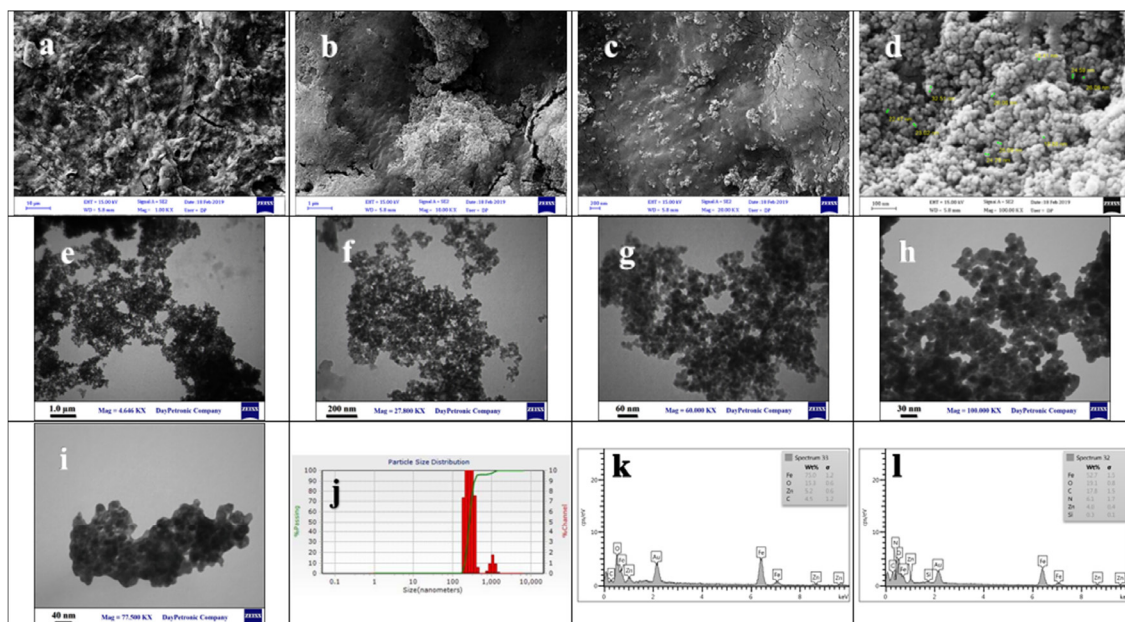


Fig. 5. SEM micrographs of ZnFe₂O₄ NPs at different magnifications; a) 1.0 μm, b) 200 nm, c) 100 nm, d) 30 nm. TEM micrographs of ZnFe₂O₄ NPs at different magnifications; e) 1.0 μm, f) 200 nm, g) 60 nm, h) 30 nm. TEM micrographs of chitosan-coated ZnFe₂O₄ NPs; i) 40 nm. DLS curve of ZnFe₂O₄ NPs; (j). EDS pattern of ZnFe₂O₄ NPs (k) and chitosan-coated ZnFe₂O₄ NPs (l).

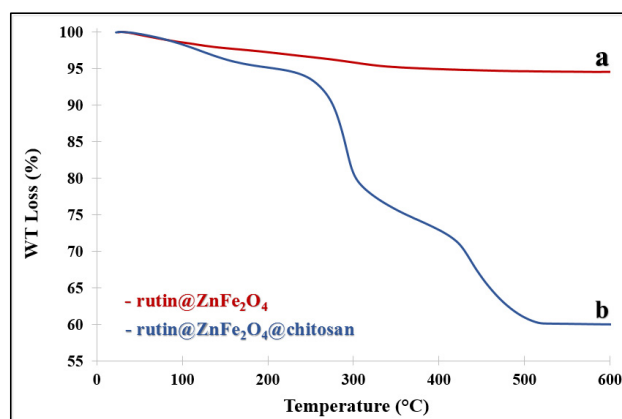


Fig. 6. TGA curves of ZnFe₂O₄ NPs (a) and chitosan-coated ZnFe₂O₄ NPs (b).

to the steric barrier of chitosan playing as the stabilizing agent [26]. The same results were also obtained by Ignat *et al.*, which the ZnFe₂O₄ NPs synthesized by the chemical method were coagulated and rod type with average size was 23.9 nm. By the way, coating by chitosan as a stabilizer has significantly decreased the size of ZnFe₂O₄ NPs [31]. The Dynamic Light Scattering (DLS) image (Fig. 5j) represents that the mean particle size diameter of the hydrogel beads (biosynthesized ZnFe₂O₄ NPs) are about 267.9 nm. In case of purity and elemental composition of rutin-ZnFe₂O₄ NPs and chitosan-coated ZnFe₂O₄ NPs, the analysis of en-

ergy dispersive X-ray spectroscopy (EDS) was applied. As can be seen in figures 5k and 5l, the EDS patterns obviously showed that biosynthesized ZnFe₂O₄ NPs either with or without chitosan were completely free from any kind of elemental impurities. The obtained results were in agreement with the chemical synthesis of ZnFe₂O₄ NPs carried out by Dhiman *et al.* [32].

TGA analysis

Fig. 6 illustrates the TGA curves of biosynthesized ZnFe₂O₄ NPs and chitosan-coated ZnFe₂O₄ NPs. For ZnFe₂O₄ NPs (Fig. 6a), the weight

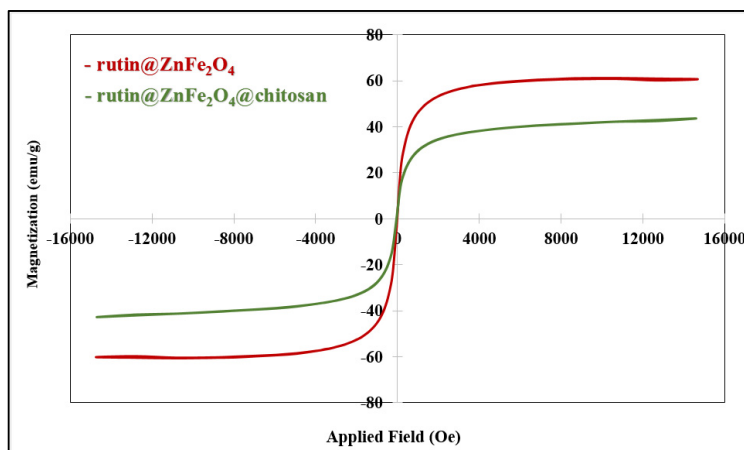


Fig. 7. Magnetic curves of ZnFe_2O_4 NPs and chitosan-coated ZnFe_2O_4 NPs.

loss is 5.5 wt.%, which it might be due to the removal extra water. On the other hand, in Fig. 6b, the dramatic weight loss is observed for the chitosan-coated ZnFe_2O_4 NPs, especially from 270°C to 500°C reaching to the 60.7 wt.%, representing the elimination of rutin and coating agent, chitosan. Afterwards, the curve experiences the linear pattern, which is more likely attributed to the pure zinc ferrite during the temperature range. The present data was also obtained as similar as the study of ZnFe_2O_4 NPs synthesized by the chemical method [26].

VSM analysis

The magnetic hysteresis loops for the biosynthesized ZnFe_2O_4 NPs as well as chitosan-coated ZnFe_2O_4 NPs are exhibited in Fig. 7. The magnetic properties of the zinc ferrite were evaluated by room temperature vibrating sample magnetometer (VSM) with a used ± 15 kOe field. The evident properties, which are extracted from the curves, are the zero coercivity along with the ferromagnetism attitude of ZnFe_2O_4 NPs in both samples. The phenomena can be regarded with the reducing of superexchange interaction between Fe^{3+} cations in the octahedral and tetrahedral sites [33]. As can be seen by the curves, the value of saturation magnetization (M_s) of 59.2 emu/g for ZnFe_2O_4 NPs was higher than that of 38.7 emu/g for chitosan-coated ZnFe_2O_4 NPs, which are different from those of reported previously. Chitosan coating decreases the magnetization value corresponding the presence of carboxylate anion ($-\text{COO}^-$) on the surface of ZnFe_2O_4 NPs, which are

produced the magnetic dead layer. Raeisi Sahraki *et al.* also reported that the magnetization of zinc ferrite magnetite declined from 7.3 emu/g to 5.2 emu/g due to the presence of chitosan as a coating agent [26]. It is worth nothing that the meaningful magnetic results of pure ZnFe_2O_4 NPs with ZnFe_2O_4 -chitosan-Folic acid-DOX-HCl nanoparticles were overlapped with the present study [34].

Electrochemical procedure and in vitro load/release of DOX

Doxorubicin concentrations show a linear calibration curve between 0.03 to 1.5 μM . Well-defined voltammetric peaks are observed at $E_p = -0.55$ V (Fig. 8).

Doxorubicin Loading

To determine the extent of drug loading, the supernatant of the centrifuged solution was collected and the amount of DOX in solution was measured by SWV. In order to specify the concentration of the drug, the recorded absorption intensity was compared with a calibration curve that was plotted for DOX. In line with the Esmaili and Hadad study, the drug loading capacity (DLC) and drug loading efficiency (DLE) parameters of the chitosan-coated ZnFe_2O_4 NPs carrier were measured as 43.5% and 78.6% [34].

Doxorubicin Release

The rate of drug release from the chitosan beads was compared at different pH values (Fig. 9). The release behavior of rutin- ZnFe_2O_4 -chitosan-DOX in the acidic PBS solution (pH 6.4;

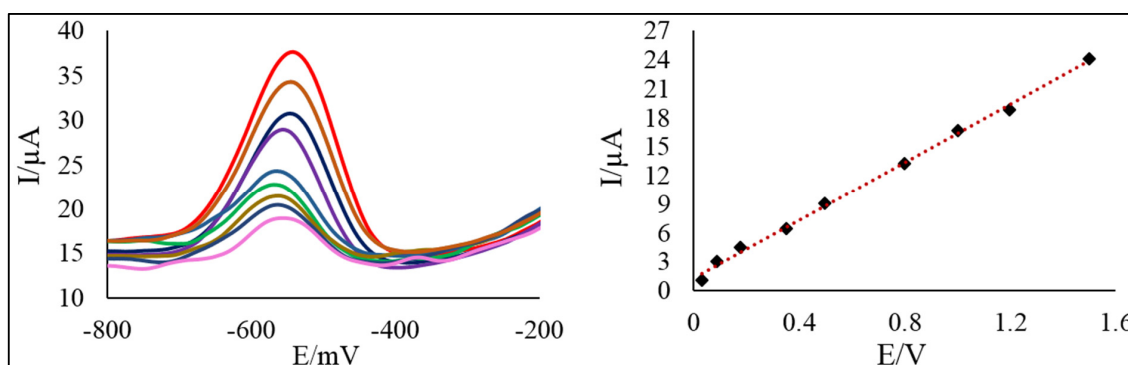


Fig. 8. A) Square-wave voltammograms (SWV) of doxorubicin at different concentrations. (B) The corresponding calibration plot. The experimental conditions include; scan from -0.2 V to -0.8 V using pulse 80 mV; scan rate 200 mV/s.

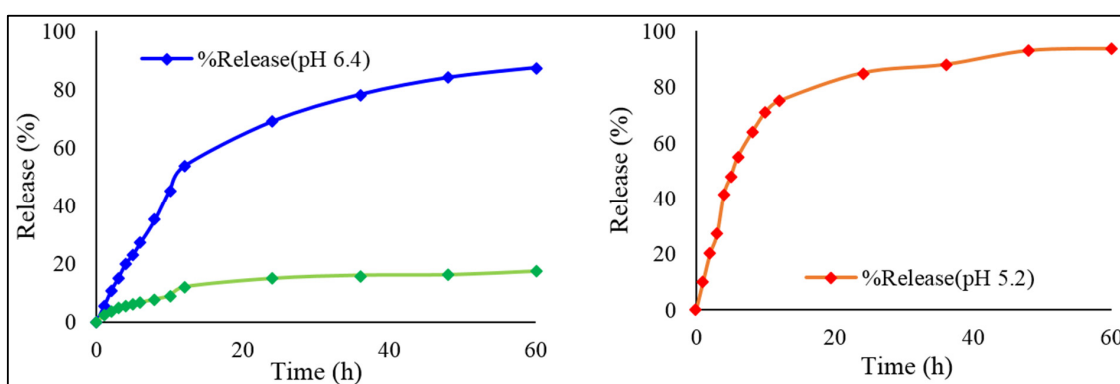


Fig. 9. Profiles of DOX release from the chitosan-coated $ZnFe_2O_4$ NPs drug delivery systems; A) at pH= 7.4 and 6.4, B) at pH=5.2

the blue line) shows a significantly faster release (87.4% within 60 h) relative to the buffer with pH 7.4 (the green graph), which indicates just 17.3% DOX release in the first 60 h. The obtained results at pH 5.2 are also studied. According to this figure, the rate of DOX release from chitosan-coated $ZnFe_2O_4$ NPs is significantly higher at pH 5.2 relative to pH 6.4.

CONCLUSION

A main objective of cancer therapy is the possibility to selectively target cancer cell while do not affect healthy cells. To the best of our knowledge, the synthesis of chitosan-coated $ZnFe_2O_4$ -doxorubicin NPs and their capacity of drug delivery was successively investigated by a glycosylated flavonoid, rutin. Rutin, a phenolic compound derived from plant extract, has been proven to be an effective reductant to the size of various nanoparticles. During the synthesis of rutin- $ZnFe_2O_4$ NPs, the substantial novelty was eliminating the N_2 gas from the process. The structural properties of the

synthesized NPs were comprehensively studied with FTIR, XRD, TEM, SEM, TGA, and VSM techniques. Capacity and efficiency parameters of the anti-cancer drug onto the NPs were obtained as equal to 43.5% and 78.6%. TEM experiment revealed that the average particle size of NPs was 18-32 nm. It is therefore found that releasing drug was more efficient in pH 6.4 rather than that of two other pHs, 7.4 and 5.2. Accordingly, the worthwhile properties of these NPs could be a golden line to further deep investigations. A comprehensive analysis of biocompatibility and toxicity of chitosan-coated $ZnFe_2O_4$ -doxorubicin NPs should be done using appropriate cell lines based *in vitro* models and consequently *in vivo* animal models, using the standardized protocols. Besides, future research is warranted to validate the findings of the present study.

ACKNOWLEDGMENTS

The authors kindly thank to Shiraz University of Medical Sciences for technical support of the

study. Research reported in this publication was supported by Elite Researcher Grant Committee under award number [987602] from the National Institute for Medical Research Development (NI-MAD), Tehran, Iran.

CONFLICT OF INTEREST

The authors declare that there is no conflict of interests regarding the publication of this manuscript.

REFERENCES

1. Virkutyte J, Varma RS. CHAPTER 2. Environmentally Friendly Preparation of Metal Nanoparticles. Green Chemistry Series: Royal Society of Chemistry; 2012. p. 7-33.
2. Christian P, Von der Kammer F, Baalousha M, Hofmann T. Nanoparticles: structure, properties, preparation and behaviour in environmental media. *Ecotoxicology*. 2008;17(5):326-43.
3. Saif S, Tahir A, Chen Y. Green Synthesis of Iron Nanoparticles and Their Environmental Applications and Implications. *Nanomaterials*. 2016;6(11):209.
4. Naseri MG, Saion EB, Hashim M, Shaari AH, Ahangar HA. Synthesis and characterization of zinc ferrite nanoparticles by a thermal treatment method. *Solid State Communications*. 2011;151(14-15):1031-5.
5. Bardhan A, Ghosh CK, Mitra MK, Das GC, Mukherjee S, Chattopadhyay KK. Low temperature synthesis of zinc ferrite nanoparticles. *Solid State Sciences*. 2010;12(5):839-44.
6. Hervault A, Dunn AE, Lim M, Boyer C, Mott D, Maenosono S, et al. Doxorubicin loaded dual pH- and thermo-responsive magnetic nanocarrier for combined magnetic hyperthermia and targeted controlled drug delivery applications. *Nanoscale*. 2016;8(24):12152-61.
7. Jeseentharani V, George M, Jeyaraj B, Dayalan A, Nagaraja KS. Synthesis of metal ferrite (MFe_2O_4 , M = Co, Cu, Mg, Ni, Zn) nanoparticles as humidity sensor materials. *Journal of Experimental Nanoscience*. 2013;8(3):358-70.
8. Morrison SA, Cahill CL, Carpenter EE, Calvin S, Swaminathan R, McHenry ME, et al. Magnetic and structural properties of nickel zinc ferrite nanoparticles synthesized at room temperature. *Journal of Applied Physics*. 2004;95(11):6392-5.
9. Park JH, Saravanakumar G, Kim K, Kwon IC. Targeted delivery of low molecular drugs using chitosan and its derivatives. *Advanced Drug Delivery Reviews*. 2010;62(1):28-41.
10. Rinaudo M. Chitin and chitosan: Properties and applications. *Progress in Polymer Science*. 2006;31(7):603-32.
11. Liang Y, Zhao X, Ma PX, Guo B, Du Y, Han X. pH-responsive injectable hydrogels with mucosal adhesiveness based on chitosan-grafted-dihydrocaffeic acid and oxidized pullulan for localized drug delivery. *Journal of Colloid and Interface Science*. 2019;536:224-34.
12. Zhang P, Kong J. Doxorubicin-tethered fluorescent silica nanoparticles for pH-responsive anticancer drug delivery. *Talanta*. 2015;134:501-7.
13. Yamaura M, Camilo RL, Sampaio LC, Macêdo MA, Nakamura M, Toma HE. Preparation and characterization of (3-aminopropyl)triethoxysilane-coated magnetite nanoparticles. *Journal of Magnetism and Magnetic Materials*. 2004;279(2-3):210-7.
14. Chandra Hembram K, Prabha S, Chandra R, Ahmed B, Nimesh S. Advances in preparation and characterization of chitosan nanoparticles for therapeutics. *Artificial Cells, Nanomedicine, and Biotechnology*. 2014;44(1):305-14.
15. Naveen P, Lingaraju HB, Anitha, Prasad K. Simultaneous determination of rutin, isoquercetin, and quercetin flavonoids in *Nelumbo nucifera* by high-performance liquid chromatography method. *International Journal of Pharmaceutical Investigation*. 2017;7(2):94.
16. Blunder M, Orthaber A, Bauer R, Bucar F, Kunert O. Efficient identification of flavones, flavanones and their glycosides in routine analysis via off-line combination of sensitive NMR and HPLC experiments. *Food Chemistry*. 2017;218:600-9.
17. Hafez Ghoran S, Fadaei Dashti M, Maroofi A, Shafiee M, Zare-Hoseinabadi A, Behzad F, et al. Biosynthesis of Zinc Ferrite Nanoparticles Using Polyphenol-rich extract of *Citrus aurantium* flowers. *Nanomedicine Research Journal*. 2020;5(1):20-28.
18. Frank LA, Onzi GR, Morawski AS, Pohlmann AR, Guterres SS, Contri RV. Chitosan as a coating material for nanoparticles intended for biomedical applications. *Reactive and Functional Polymers*. 2020;147:104459.
19. Polat O. Controlled Molecular Release from Nanoporous Gold Thin Films: University of California, Davis; 2016.
20. Mozaffarian V. A dictionary of Iranian plant names 2003.
21. Janbaz KH, Saeed SA, Gilani AH. Protective effect of rutin on paracetamol- and CCl_4 -induced hepatotoxicity in rodents. *Fitoterapia*. 2002;73(7-8):557-63.
22. Aherne SA, O'Brien NM. Mechanism of protection by the flavonoids, quercetin and rutin, against tert-butylhydroperoxide- and menadione-induced DNA single strand breaks in Caco-2 cells. *Free Radical Biology and Medicine*. 2000;29(6):507-14.
23. Ikeda NEA, Novak EM, Maria DA, Velosa AS, Pereira RMS. Synthesis, characterization and biological evaluation of Rutin-zinc(II) flavonoid-metal complex. *Chemico-Biological Interactions*. 2015;239:184-91.
24. Fernandes Queiroz M, Melo K, Sabry D, Sasaki G, Rocha H. Does the Use of Chitosan Contribute to Oxalate Kidney Stone Formation? *Marine Drugs*. 2014;13(1):141-58.
25. Lima VVC, Dalla Nora FB, Peres EC, Reis GS, Lima EC, Oliveira MLS, et al. Synthesis and characterization of biopolymers functionalized with APTES (3-aminopropyltriethoxysilane) for the adsorption of sunset yellow dye. *Journal of Environmental Chemical Engineering*. 2019;7(5):103410.
26. Raeisi Shahraki R, Seyyed Ebrahim SA, Masoudpanah SM. Synthesis and Characterization of Superparamagnetic Zinc Ferrite-Chitosan Composite Nanoparticles. *Journal of Superconductivity and Novel Magnetism*. 2015;28(7):2143-7.
27. Raeisi Shahraki R, Ebrahimi M. Synthesize of superparamagnetic zinc ferrite nanoparticles at room temperature. *Journal of Nanostructures*. 2012;2(4):413-416.
28. Waldron RD. Infrared Spectra of Ferrites. *Physical Review*. 1955;99(6):1727-35.
29. Najafi Birgani A, Niyafar M, Hasanpour A. Study of cation distribution of spinel zinc nano-ferrite by X-ray. *Journal of Magnetism and Magnetic Materials*. 2015;374:179-81.
30. Holzwarth U, Gibson N. The Scherrer equation versus

- the 'Debye-Scherrer equation'. *Nature Nanotechnology*. 2011;6(9):534-.
31. Ignat M, Samoila P, Cojocar C, Sacarescu L, Harabagiu V. Novel Synthesis Route for Chitosan-Coated Zinc Ferrite Nanoparticles as Potential Sorbents for Wastewater Treatment. *Chemical Engineering Communications*. 2016;203(12):1591-9.
 32. Dhiman M, Sharma R, Kumar V, Singhal S. Morphology controlled hydrothermal synthesis and photocatalytic properties of ZnFe₂O₄ nanostructures. *Ceramics International*. 2016;42(11):12594-605.
 33. Chinnasamy CN, Narayanasamy A, Ponpandian N, Chattopadhyay K. The influence of Fe³⁺ ions at tetrahedral sites on the magnetic properties of nanocrystalline ZnFe₂O₄. *Materials Science and Engineering: A*. 2001;304-306:983-7.
 34. Esmaeili A, Alizadeh Hadad N. Preparation of ZnFe₂O₄-chitosan-doxorubicin hydrochloride nanoparticles and investigation of their hyperthermic heat-generating characteristics. *Ceramics International*. 2015;41(6):7529-35.